particles

MDPI

Article

Bulk Viscosity of Hot Quark Plasma from Non-Equilibrium Statistical Operator

Arus Harutyunyan [1,*] and Armen Sedrakian [2]

[1] Institute for Theoretical Physics, Goethe University, Max-von-Laue-Straße, 1, 60438 Frankfurt am Main, Germany
[2] Frankfurt Institute for Advanced Studies, Ruth-Moufang-Straße, 1, 60438 Frankfurt am Main, Germany; sedrakian@fias.uni-frankfurt.de
* Correspondence: arus@th.physik.uni-frankfurt.de; Tel.:+49-069-798-47691

Received: 18 June 2018; Accepted: 13 August 2018; Published: 20 August 2018

Abstract: We provide a discussion of the bulk viscosity of two-flavor quark plasma, described by the Nambu–Jona-Lasinio model, within the framework of Kubo-Zubarev formalism. This discussion, which is complementary to our earlier study, contains a new, detailed derivation of the bulk viscosity in the case of multiple conserved charges. We also provide some numerical details of the computation of the bulk viscosity close to the Mott transition line, where the dissipation is dominated by decays of mesons into quarks and their inverse processes. We close with a summary of our current understanding of this quantity, which stresses the importance of loop resummation for obtaining the qualitatively correct result near the Mott line.

Keywords: transport coefficients; bulk viscosity; correlation functions; statistical operator

1. Introduction

Transport coefficients of hot and dense quark plasma are key inputs in the hydrodynamical description of the heavy-ion experiments at Relativistic Heavy Ion Collider (RHIC) and Large Hadron Collider (LHC). The matter created in these experiments exhibits a very small ratio of the shear viscosity to the entropy density, which is close to the lower bound placed by the uncertainty principle [1] and conjectured on the basis of AdS/CFT duality [2].

The bulk viscosity describes the dissipation in cases where pressure falls out of its equilibrium value on uniform expansion or contraction of fluid. It vanishes in several cases, e.g., for an ultrarelativistic or nonrelativistic gas interacting weakly with local forces via binary collisions, as well as in strongly coupled systems with conformal symmetry. Because at high energies QCD is almost conformally symmetric, the bulk viscosity of quark-gluon plasma is small in the perturbative regime [3–6]. At low energies, the conformal symmetry is broken by the quark mass and/or by dimensionful regularization of the ultraviolet divergences, in which case the bulk viscous effects can become important. Large values of bulk viscosity were found, in particular, close to the chiral phase transition line [7,8]. Computations of the QCD bulk viscosity in the strongly coupled regime where carried out using various methods including lattice simulations [5,9,10], quasiparticle Boltzmann transport [11–15] and the Kubo formalism [16–18].

The focus of this contribution, which is complementary to our earlier study [16], is the bulk viscosity of quark matter in the non-perturbative regime as it is realized close to the chiral phase transition line. The case of bulk viscosity is special because it requires a resummation of an infinite series of loop diagrams, whereas the remaining coefficient (shear viscosity, thermal and electrical conductivities) are given by the one-loop result only, see Ref. [19]. Specifically, our aim here is to provide details of the computation of this quantity which complement our earlier publication [16]. First, we provide a formal derivation of the bulk viscosity coefficient from the Zubarev formalism of

non-equilibrium statistical operator (NESO) [20,21] in a general setting of relativistic quantum field theory assuming a system with multiple conserved charges. We then go on to discuss the details of diagrammatic evaluation of the bulk viscosity within the Nambu–Jona-Lasinio (NJL) model, which is an effective field theory of QCD that captures its chiral symmetry breaking feature. The main mechanism of dissipation within this model is provided by the mesonic fluctuations close to the critical line of chiral phase transition.

Another important ingredient of the diagrammatic evaluation of the two-point correlation function determining the bulk viscosity is the $1/N_c$ expansion [22]. Several recent computations of bulk viscosity, which were based on a Kubo formula and the NJL model, evaluated the relevant correlation function at the one-loop level [17,18]. However, our recent analysis [16] indicates, that the one-loop approximation is not consistent with the $1/N_c$ power counting scheme and a resummation of infinite series of loop diagrams is required to obtain the leading-order approximation to the bulk viscosity. Below, we provide some numerical details of this computation.

This work is organized as follows. In Section 2 we review Zubarev's method of the NESO and derive a Kubo-type formula for the bulk viscosity. Section 3 is devoted to the application of the general formalism to the case of two-flavor quark matter described by the NJL model. Our numerical results for the bulk viscosity are collected in Section 4. Section 5 provides a short summary. The computation of a Matsubara sum, which is used in the derivation of the Kubo formula, is relegated to Appendix A. We use the natural (Gaussian) units with $\hbar = c = k_B = 1$, and the metric signature $g^{\mu\nu} = \mathrm{diag}(1, -1, -1, -1)$.

2. Bulk Viscosity Formula from the Non-Equilibrium Statistical Operator

The coefficient of the bulk viscosity was computed within the NESO method for the case of a system without conserved charges in the seminal paper by Hosoya et al. [23]. Our purpose here is to extend that derivation to the case of systems with multiple conserved charges.

Hydrodynamics of relativistic quantum fluids is described by the energy-momentum tensor $\hat{T}^{\mu\nu}(x)$ and currents of conserved charges $\hat{N}^{\mu}_a(x)$. We consider the general case of multiple conserved charge flavors (e.g., baryonic, electric, etc.) which are labeled by the index a. In this case, these conservation laws take the form

$$\partial_\mu \hat{T}^{\mu\nu}(x) = 0, \qquad \partial_\mu \hat{N}^{\mu}_a(x) = 0. \tag{1}$$

For systems in the hydrodynamic regime, one can introduce local thermodynamic variables, such as temperature $T(x) \equiv \beta^{-1}(x)$, chemical potentials $\mu_a(x)$ and fluid 4-velocity $u^\nu(x)$ as smooth functions of the space-time coordinates $x \equiv (\boldsymbol{x}, t)$. Below we will specify the (matching) conditions which are necessary to identify these quantities. Our next step is to define a NESO as

$$\hat{\rho}(t) = Q^{-1} e^{-\hat{A}+\hat{B}}, \qquad Q = \mathrm{Tr} e^{-\hat{A}+\hat{B}}, \tag{2}$$

with operators defined as

$$\hat{A}(t) = \int d^3x \Big[\beta^\nu(x)\hat{T}_{0\nu}(x) - \sum_a \alpha_a(x)\hat{N}^0_a(x)\Big], \tag{3}$$

$$\hat{B}(t) = \lim_{\varepsilon\to+0} \int d^3x_1 \int_{-\infty}^{t} dt_1 e^{\varepsilon(t_1-t)} \hat{C}(x_1), \tag{4}$$

$$\hat{C}(x) = \hat{T}_{\mu\nu}(x)\partial^\mu\beta^\nu(x) - \sum_a \hat{N}^\mu_a(x)\partial_\mu\alpha_a(x), \tag{5}$$

where the covariant quantities (c-numbers) are defined as

$$\beta^\nu(x) = \beta(x)u^\nu(x), \qquad \alpha_a(x) = \beta(x)\mu_a(x). \tag{6}$$

Note that the limit $\varepsilon \to +0$ in Equation (4) should be taken only after the thermodynamic limit. The proper order of taking the thermodynamic and $\varepsilon \to +0$ limits guarantees that the NESO in Equation (2) satisfies the Liouville equation with an infinitesimal source term, which breaks the time-reversibility of that equation and chooses its retarded solution for positive values of ε [20,21,23]. Equations (2)–(6) generalize the analogous expressions of Refs. [23,24] to the case of a system with multiple conserved charges.

The first term in the exponent in Equation (2) corresponds to the local equilibrium part of the statistical operator, defined as

$$\hat{\rho}_l(t) = Q_l^{-1} e^{-\hat{A}}, \qquad Q_l = \mathrm{Tr} e^{-\hat{A}}. \tag{7}$$

The second term in the exponent of Equation (2) is the non-equilibrium part of the statistical operator, which can be interpreted as a thermodynamic "force". For small deviations from equilibrium, it can be treated as a small perturbation. Expanding the NESO around the local equilibrium distribution and keeping linear in the operator $\hat{B}$ terms we find

$$\hat{\rho} = \left[1 + \int_0^1 d\tau \left(e^{-\tau\hat{A}} \hat{B} e^{\tau\hat{A}} - \langle \hat{B} \rangle_l\right)\right] \hat{\rho}_l. \tag{8}$$

The statistical average of any operator $\hat{X}(x)$ can be written now as

$$\langle \hat{X}(x) \rangle = \mathrm{Tr}[\hat{\rho}(t)\hat{X}(x)] = \langle \hat{X}(x) \rangle_l + \int d^3x_1 \int_{-\infty}^{t} dt_1 e^{\varepsilon(t_1 - t)} \left(\hat{X}(x), \hat{C}(x_1)\right), \tag{9}$$

where $\langle \hat{X}(x) \rangle_l$ is the local equilibrium average and a two-point correlation function has been defined as [23,24]

$$\left(\hat{X}(x), \hat{C}(x_1)\right) = \int_0^1 d\tau \langle \hat{X}(x) \left[e^{-\tau\hat{A}} \hat{C}(x_1) e^{\tau\hat{A}} - \langle \hat{C}(x_1) \rangle_l\right] \rangle_l. \tag{10}$$

The final point of our general discussion of the NESO method is the procedure by which the quantities β^ν and α_a are matched with the relevant thermodynamic variables in an arbitrary non-equilibrium state. This can be achieved by the following *matching conditions* [20,21,24]

$$\langle \hat{\epsilon}(x) \rangle = \langle \hat{\epsilon}(x) \rangle_l, \qquad \langle \hat{n}_a(x) \rangle = \langle \hat{n}_a(x) \rangle_l, \tag{11}$$

where the operators of the energy and charge densities are defined as $\hat{\epsilon} = u_\mu u_\nu \hat{T}^{\mu\nu}$ and $\hat{n}_a = u_\mu \hat{N}_a^\mu$. In these expressions, the fluid 4-velocity u^μ, which is normalized to unity $u_\mu u^\mu = 1$, should be "tied" to a physical current. This could be either the energy flow, which specifies the Landau-Lifshitz frame [25] or the charge flow, which specifies the Eckart frame [26]. In the Landau frame $u_\mu \langle \hat{T}^{\mu\nu} \rangle = \langle \hat{\epsilon} \rangle u^\nu$, whereas in the Eckart frame $\langle \hat{N}_a^\mu \rangle = \langle \hat{n}_a \rangle u^\mu$. The conditions (11) define the temperature and the chemical potentials of components as *non-local functionals* of $\langle \hat{\epsilon}(x) \rangle$ and $\langle \hat{n}_a(x) \rangle$ [27]. However, the hydrodynamic description requires thermodynamic parameters as *local* functions of the energy and charge densities. In practice, this difficulty is circumvented by dividing the fluid into elements which are in local statistical equilibrium and each of which is independent of the other [28]. In practice, the local equilibrium values $\langle \hat{\epsilon} \rangle_l$ and $\langle \hat{n}_a \rangle_l$ in Equation (11) are then evaluated assuming formally *constant values* of β and μ_a, which are identified by matching $\langle \hat{\epsilon} \rangle_l$ and $\langle \hat{n}_a \rangle_l$ to the real values of these quantities $\langle \hat{\epsilon} \rangle$ and $\langle \hat{n}_a \rangle$ at any given point x. In this way one can construct a *fictitious local equilibrium state*, characterized by the thermodynamic parameters $\beta(x)$ and $\mu_a(x)$, such that it reproduces the local values of the energy and charge densities at every point of the space and time.

2.1. Decomposition into Different Dissipative Processes

To identify the different dissipative processes, we now exploit the common decompositions of the energy-momentum tensor and the charge currents into the ideal and dissipative parts

$$\hat{T}^{\mu\nu} = \hat{\epsilon} u^\mu u^\nu - \hat{p}\Delta^{\mu\nu} + \hat{q}^\mu u^\nu + \hat{q}^\nu u^\mu + \hat{\pi}^{\mu\nu}, \tag{12}$$

$$\hat{N}^\mu_a = \hat{n}_a u^\mu + \hat{j}^\mu_a, \tag{13}$$

where $\hat{p}$ is the operator of pressure; $\Delta^{\mu\nu} = g^{\mu\nu} - u^\mu u^\nu$ is the projection operator onto the 3-space orthogonal to u_μ and has the properties

$$u_\mu \Delta^{\mu\nu} = \Delta^{\mu\nu} u_\nu = 0, \qquad \Delta^{\mu\nu}\Delta_{\nu\lambda} = \Delta^\mu_\lambda, \qquad \Delta^\mu_\mu = 3. \tag{14}$$

The dissipative quantities $\hat{\pi}^{\mu\nu}$, $\hat{q}^\mu$ and $\hat{j}^\mu_a$ are the operators of the shear stress tensor, energy diffusion flux and charge diffusion fluxes, respectively, and they satisfy the following conditions

$$u_\nu \hat{q}^\nu = 0, \qquad u_\nu \hat{j}^\nu_a = 0, \qquad u_\nu \hat{\pi}^{\mu\nu} = 0, \qquad \hat{\pi}^\mu_\mu = 0. \tag{15}$$

The operators on the right-hand sides of Equations (12) and (13) can be obtained via the projections of $\hat{T}^{\mu\nu}$ and $\hat{N}^\mu_a$

$$\hat{\epsilon} = u_\mu u_\nu \hat{T}^{\mu\nu}, \qquad \hat{n}_a = u_\mu \hat{N}^\mu_a, \qquad \hat{p} = -\frac{1}{3}\Delta_{\mu\nu}\hat{T}^{\mu\nu}, \tag{16}$$

$$\hat{\pi}^{\mu\nu} = \Delta^{\mu\nu}_{\alpha\beta}\hat{T}^{\alpha\beta}, \qquad \hat{q}^\mu = u_\alpha \Delta^\mu_\beta \hat{T}^{\alpha\beta}, \qquad \hat{j}^\nu_a = \Delta^\nu_\mu \hat{N}^\mu_a, \tag{17}$$

which in the local rest frame $[u_\mu = (1,0,0,0)]$ read

$$\hat{\epsilon} = \hat{T}^{00}, \qquad \hat{n}_a = \hat{N}^0_a, \qquad \hat{p} = -\frac{1}{3}\hat{T}^k_k, \tag{18}$$

$$\hat{\pi}_{kl} = \left(\delta_{ki}\delta_{lj} - \frac{1}{3}\delta_{kl}\delta_{ij}\right)\hat{T}_{ij}, \qquad \hat{q}^i = \hat{T}^{0i}, \qquad \hat{j}^i_a = \hat{N}^i_a. \tag{19}$$

In Equation (17) we introduced a fourth-rank traceless projector orthogonal to u^μ

$$\Delta_{\mu\nu\rho\sigma} = \frac{1}{2}\left(\Delta_{\mu\rho}\Delta_{\nu\sigma} + \Delta_{\mu\sigma}\Delta_{\nu\rho}\right) - \frac{1}{3}\Delta_{\mu\nu}\Delta_{\rho\sigma}. \tag{20}$$

The hydrodynamic quantities $\pi^{\mu\nu}$, q^μ and j^μ_a are obtained as the statistical averages of the corresponding operators over the NESO according to Equations (9) and (10). In local equilibrium the averages of the dissipative operators vanish:

$$\langle \hat{q}^\mu \rangle_l = 0, \qquad \langle \hat{j}^\mu \rangle_l = 0, \qquad \langle \hat{\pi}^{\mu\nu} \rangle_l = 0. \tag{21}$$

To compute the non-equilibrium averages of these operators it is convenient to write the operator $\hat{C}$ given by Equation (5) as a sum of contributions of different dissipative processes according to Equations (12) and (13). Similar decompositions were performed in Refs. [23,24]. Recalling the properties (14) and (15) we obtain

$$\hat{C} = \hat{\epsilon} D\beta - \hat{p}\beta\theta - \sum_a \hat{n}_a D\alpha_a + \hat{q}^\lambda(\beta D u_\lambda + \nabla_\lambda \beta) - \sum_a \hat{j}^\lambda_a \nabla_\lambda \alpha_a + \beta \hat{\pi}_{\lambda\rho}\sigma^{\lambda\rho}, \tag{22}$$

where we introduced the covariant time-derivative $D = u^\rho \partial_\rho$, the covariant spatial derivative $\nabla_\rho = \Delta_{\rho\lambda}\partial^\lambda$, the fluid expansion rate $\theta = \partial_\rho u^\rho$ and the velocity stress tensor via $\sigma^{\lambda\rho} = \Delta^{\lambda\rho\alpha\beta}\partial_\alpha u_\beta$.

As a first approximation, we can eliminate the terms $D\beta$, $D\alpha_a$ and Du_λ using the equations of ideal hydrodynamics

$$Dn_a + n_a\theta = 0, \qquad D\epsilon + h\theta = 0, \qquad hDu_\lambda = \nabla_\lambda p, \tag{23}$$

where $p = p(\epsilon, n_a)$ is the equilibrium pressure fixed by an equation of state, and $h = \epsilon + p$ is the enthalpy density. Choosing ϵ and n_a as independent thermodynamic variables and using the first two equations in (23) we can write

$$D\beta = \left(\frac{\partial\beta}{\partial\epsilon}\right)_{n_a} D\epsilon + \sum_a \left(\frac{\partial\beta}{\partial n_a}\right)_{\epsilon, n_b\neq n_a} Dn_a = -h\theta\left(\frac{\partial\beta}{\partial\epsilon}\right)_{n_a} - \sum_a n_a\theta\left(\frac{\partial\beta}{\partial n_a}\right)_{\epsilon, n_b\neq n_a}, \tag{24}$$

$$D\alpha_c = \left(\frac{\partial\alpha_c}{\partial\epsilon}\right)_{n_a} D\epsilon + \sum_a \left(\frac{\partial\alpha_c}{\partial n_a}\right)_{\epsilon, n_b\neq n_a} Dn_a = -h\theta\left(\frac{\partial\alpha_c}{\partial\epsilon}\right)_{n_a} - \sum_a n_a\theta\left(\frac{\partial\alpha_c}{\partial n_a}\right)_{\epsilon, n_b\neq n_a}. \tag{25}$$

In the next step we exploit the thermodynamic relations

$$ds = \beta d\epsilon - \sum_a \alpha_a dn_a, \qquad \beta dp = -hd\beta + \sum_a n_a d\alpha_a, \tag{26}$$

to obtain

$$\left(\frac{\partial\beta}{\partial n_a}\right)_{\epsilon, n_b\neq n_a} = -\left(\frac{\partial\alpha_a}{\partial\epsilon}\right)_{n_b}, \qquad \left(\frac{\partial\alpha_c}{\partial n_a}\right)_{\epsilon, n_b\neq n_a} = \left(\frac{\partial\alpha_a}{\partial n_c}\right)_{\epsilon, n_b\neq n_c}, \tag{27}$$

$$h = -\beta\left(\frac{\partial p}{\partial\beta}\right)_{\alpha_a}, \qquad n_a = \beta\left(\frac{\partial p}{\partial\alpha_a}\right)_{\beta, \alpha_b\neq\alpha_a}. \tag{28}$$

Substituting these relations back into Equations (24) and (25) we obtain

$$D\beta = \beta\theta\left(\frac{\partial p}{\partial\epsilon}\right)_{n_a}, \qquad D\alpha_c = -\beta\theta\left(\frac{\partial p}{\partial n_c}\right)_{\epsilon, n_b\neq n_c}. \tag{29}$$

Now the first three terms in Equation (22) can be combined as follows

$$\hat{\epsilon}D\beta - \hat{p}\beta\theta - \sum_a \hat{n}_a D\alpha_a = -\beta\theta\hat{p}^*, \tag{30}$$

where

$$\hat{p}^* = \hat{p} - \left(\frac{\partial p}{\partial\epsilon}\right)_{n_a}\hat{\epsilon} - \sum_a \left(\frac{\partial p}{\partial n_a}\right)_{\epsilon, n_b\neq n_a}\hat{n}_a. \tag{31}$$

2.2. Kubo Formula for the Bulk Viscosity

By definition, bulk viscous pressure Π measures the deviation of the thermodynamic pressure from its equilibrium value, which results from the expansion or compression of the fluid. Therefore, it might appear at a first glance that the bulk viscous pressure should be identified as $\langle\hat{p}\rangle - \langle\hat{p}\rangle_l$. However, it is easy to see that such a definition would be erroneous. To understand the problem, we go back to the matching conditions (11), which define the local equilibrium state. As explained above, these conditions are satisfied only if the local equilibrium distribution function is evaluated formally assuming *uniform* background values of the thermodynamic parameters, i.e., as if these were constant in space and time with the given values $\beta(x)$ and $\mu_a(x)$. Because the local equilibrium distribution (7) is actually a functional of *non-uniform* thermodynamic parameters, the average values $\langle\hat{\epsilon}\rangle_l$ and $\langle\hat{n}_a\rangle_l$ in the full computation are shifted from the actual values of $\epsilon = \langle\hat{\epsilon}\rangle$ and $n_a = \langle\hat{n}_a\rangle$ by additional gradient terms $\Delta\epsilon \equiv \langle\hat{\epsilon}\rangle - \langle\hat{\epsilon}\rangle_l$ and $\Delta n_a \equiv \langle\hat{n}_a\rangle - \langle\hat{n}_a\rangle_l$, which were neglected in Equation (11). These shifts bring, in their turn, an additional shift in the equilibrium part of the pressure $\langle\hat{p}\rangle_l$, which should not be

included in the bulk viscous pressure [4,29,30]. Thus, the bulk viscous pressure should be defined as the difference between the actual non-equilibrium pressure $\langle \hat{p} \rangle$ and the equilibrium pressure $p(\epsilon, n_a)$, which is *not equal* to $\langle \hat{p} \rangle_l \equiv p(\langle \hat{\epsilon} \rangle_l, \langle \hat{n}_a \rangle_l)$:

$$p(\epsilon, n_a) = p(\langle \hat{\epsilon} \rangle_l + \Delta\epsilon, \langle \hat{n}_a \rangle_l + \Delta n_a) = \langle \hat{p} \rangle_l + \left(\frac{\partial p}{\partial \epsilon} \right)_{n_a} \Delta\epsilon + \sum_a \left(\frac{\partial p}{\partial n_a} \right)_{\epsilon, n_b \neq n_a} \Delta n_a, \tag{32}$$

where we kept only the linear terms. Then, the bulk viscous pressure is given by

$$\Pi \equiv \langle \hat{p} \rangle - p(\epsilon, n_a) = \langle \hat{p}^* \rangle - \langle \hat{p}^* \rangle_l, \tag{33}$$

where we used the definition of $\hat{p}^*$ given by Equation (31). From Equations (9), (22) and (30) we then obtain

$$\Pi = -\beta\theta \int d^3x_1 \int_{-\infty}^{t} dt_1 e^{\varepsilon(t_1 - t)} \Big(\hat{p}^*(x), \hat{p}^*(x_1) \Big), \tag{34}$$

where we dropped the correlators between operators of different rank, because they vanish in isotropic medium according to Curie's theorem [31]. Introducing the bulk viscosity as

$$\zeta = \beta \int d^3x_1 \int_{-\infty}^{t} dt_1 e^{\varepsilon(t_1 - t)} \Big(\hat{p}^*(x), \hat{p}^*(x_1) \Big), \tag{35}$$

we rewrite Equation (34) as

$$\Pi = -\zeta\theta. \tag{36}$$

The correlator (35) can be evaluated using uniform background values of thermodynamic parameters, i.e., as if the system is in *global thermal equilibrium*. Finally, the bulk viscosity can be cast in the form of a Kubo formula [23,24]

$$\zeta = -\frac{d}{d\omega} \mathrm{Im} G^R_\zeta(\omega) \Big|_{\omega=0}, \tag{37}$$

where the two-point retarded *equilibrium* Green's function in the zero-wavenumber limit is given by

$$G^R_\zeta(\omega) = -i \int_0^\infty dt e^{i\omega t} \int d^3x \langle \big[\hat{p}^*(\boldsymbol{x}, t), \hat{p}^*(\mathbf{0}, 0) \big] \rangle_l, \tag{38}$$

where the square brackets denote a commutator.

3. Bulk Viscosity within the Two-Flavor NJL Model

In this section, we illustrate the computation of the bulk viscosity following Ref. [16]; in doing so we will provide some numerical details not exposed earlier. The Lagrangian of the two-flavor NJL model contains scalar-isoscalar and pseudoscalar-isovector channels of interactions among quarks and is given by

$$\mathcal{L} = \bar{\psi}(i\partial\!\!\!/ - m_0)\psi + \frac{G}{2} \left[(\bar{\psi}\psi)^2 + (\bar{\psi} i\gamma_5 \boldsymbol{\tau} \psi)^2 \right], \tag{39}$$

where $\psi = (u, d)^T$ is the Dirac field for u and d quarks, $m_0 = 5.5$ MeV is the current-quark mass, $G = 10.1$ GeV^{-2} is the effective coupling and $\boldsymbol{\tau}$ is the vector of Pauli matrices in the space of isospin. The NJL model is regularized with a three-momentum cut-off $\Lambda = 0.65$ GeV. Assuming isospin-symmetry, the only conserved current is the net particle current given by

$$\hat{N}_\mu = \bar{\psi}\gamma_\mu\psi. \tag{40}$$

The energy-momentum tensor reads

$$\hat{T}_{\mu\nu} = \frac{i}{2}(\bar{\psi}\gamma_\mu\partial_\nu\psi + \bar{\psi}\gamma_\nu\partial_\mu\psi) - g_{\mu\nu}\mathcal{L}. \tag{41}$$

The relevant operator $\hat{p}^*$ which enters the Kubo formula (37) with the correlator given by Equation (38) in the local rest frame reads (see Equations (18) and (31))

$$\hat{p}^* = \frac{1}{3}\hat{T}_{ii} - \left(\frac{\partial p}{\partial \epsilon}\right)_n \hat{T}_{00} - \left(\frac{\partial p}{\partial n}\right)_\epsilon \hat{N}_0. \tag{42}$$

Inserting Equation (42) back into Equation (38) and using the symmetry relations $[\hat{T}_{11}, \hat{T}_{22}] = [\hat{T}_{22}, \hat{T}_{11}] = [\hat{T}_{11}, \hat{T}_{33}]$, etc., we obtain

$$\begin{array}{rcl} G^R_\zeta(\omega) & = & -i\int_0^\infty dt e^{i\omega t}\int d^3x \langle \frac{1}{3}[\hat{T}_{11}, \hat{T}_{11}] + \frac{2}{3}[\hat{T}_{11}, \hat{T}_{22}] - 2\gamma[\hat{T}_{11}, \hat{T}_{00}] \\ & & -2\delta[\hat{T}_{11}, \hat{N}_0] + 2\gamma\delta[\hat{T}_{00}, \hat{N}_0] + \gamma^2[\hat{T}_{00}, \hat{T}_{00}] + \delta^2[\hat{N}_0, \hat{N}_0]\rangle_l, \end{array} \tag{43}$$

where we omitted the arguments of the operators. Substituting here the explicit expressions for $\hat{T}_{\mu\nu}$ and $\hat{N}_\mu$ and switching to the imaginary-time (Matsubara) formalism via the substitutions $t \to -i\tau$, $\partial_t \to i\partial_\tau$, we obtain

$$\begin{array}{rcl} -G^M_\zeta(\omega_n) & = & \frac{1}{3}\Pi[i\gamma_1\partial_1, i\gamma_1\partial_1] + \frac{2}{3}\Pi[i\gamma_1\partial_1, i\gamma_2\partial_2] - 2\gamma\Pi[i\gamma_1\partial_1, -\gamma_0\partial_\tau] \\ & - & 2\delta\Pi[i\gamma_1\partial_1, \gamma_0] + 2\gamma\delta\Pi[-\gamma_0\partial_\tau, \gamma_0] + \gamma^2\Pi[-\gamma_0\partial_\tau, -\gamma_0\partial_\tau] \\ & + & \delta^2\Pi[\gamma_0, \gamma_0] + 2(1+\gamma)\Pi[i\gamma_1\partial_1, i\partial\!\!\!/_\tau - m_0] - 2\gamma(1+\gamma)\Pi[-\gamma_0\partial_\tau, i\partial\!\!\!/_\tau - m_0] \\ & - & 2\delta(1+\gamma)\Pi[\gamma_0, i\partial\!\!\!/_\tau - m_0] + (1+\gamma)^2\Pi[i\partial\!\!\!/_\tau - m_0, i\partial\!\!\!/_\tau - m_0], \end{array} \tag{44}$$

with two-point correlation functions defined as

$$\Pi[\hat{a}, \hat{b}](\omega_n) = \int_0^\beta d\tau e^{i\omega_n\tau}\int d\boldsymbol{r}\langle \mathcal{T}_\tau(\bar{\psi}\hat{a}\psi\Big|_{(\boldsymbol{r},\tau)}, \bar{\psi}\hat{b}\psi\Big|_0)\rangle_0, \tag{45}$$

where $\omega_n = 2\pi nT$, $n = 0, \pm 1, \ldots$ are the bosonic Matsubara frequencies; $\mathcal{T}_\tau$ is the imaginary time-ordering operator; $i\partial\!\!\!/_\tau \equiv -\gamma_0\partial_\tau - i\gamma_j\partial_j$, and $\hat{a}$ and $\hat{b}$ are either constants or γ-matrices contracted with partial derivatives. (Note that the correlators which arise from the interaction part of Equation (39) vanish for $\omega \neq 0$ because of the energy conservation, see Ref. [16] for details). Figure 1 illustrates diagrammatically the series of the loop diagrams which contribute to the correlation function given by Equation (45).

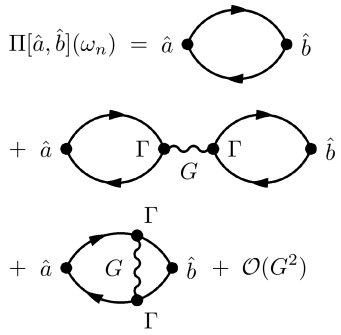

Figure 1. Contributions to the two-point correlation functions from $\mathcal{O}(N_c^1)$ (first and second lines) and $\mathcal{O}(N_c^0)$ (the third line) diagrams which are either of zeroth or first order in the coupling constant G. The interaction vertex Γ stands for the strong (scalar or pseudoscalar) vertex. The operators $\hat{a}$ and $\hat{b}$ are defined in the text.

Resummation of the Feynman Diagrams

The class of leading-order diagrams which contributes to the correlation function (45) is identified according to the $\mathcal{O}(1/N_c)$ power-counting scheme. In this scheme each diagram is selected according to its power with respect to the color number N_c, which is determined by the following rules [22]: (a) each quark loop contributes a factor of N_c, which arises from the trace over the color space; (b) each coupling G contributes a factor of $1/N_c$. It is easy to see that the leading-order diagrams in the correlation function (45) are of the order of $\mathcal{O}(N_c^1)$ and involve loop diagrams without vertex corrections, i.e., those of the type shown in the first and the second lines in Figure 1. Indeed, the factor N_c associated with each additional loop is compensated by the factor $1/N_c$ from an interaction insertion. Therefore, we conclude that we need to resume an infinite chain of loop diagrams without vertex corrections. To carry out the resummation, define the single-loop diagram in the momentum space as

$$\Pi_0[\hat{a},\hat{b}](\omega_n) = -T\sum_l \int \frac{d\boldsymbol{p}}{(2\pi)^3} \mathrm{Tr}\left[\hat{a}D(\boldsymbol{p}, i\omega_l + i\omega_n)\hat{b}D(\boldsymbol{p}, i\omega_l)\right], \tag{46}$$

where $D(\boldsymbol{p}, i\omega_l)$ is the full (i.e., dressed) quark propagator defined in the imaginary time, and the summation is over the fermionic Matsubara frequencies $\omega_l = \pi(2l+1)T - i\mu$, $l = 0, \pm 1, \ldots$, where μ is the quark chemical potential. The traces should be taken in Dirac, color, and flavor spaces. The resummation then leads to

$$\Pi[\hat{a},\hat{b}] = \Pi_0[\hat{a},\hat{b}] + \tilde{G}\Pi_0[\hat{a},\Gamma]\Pi_0[\Gamma,\hat{b}], \tag{47}$$

where $\Gamma = 1$ (the correlators with the pseudoscalar vertex $\propto \gamma_5$ vanish because the relevant traces vanish in the Dirac space). The frequency arguments in Equation (47) were omitted for the sake of brevity. The effective coupling in Equation (47) is related to the bare coupling G via

$$\tilde{G}(\omega_n) = \frac{G}{1 - G\Pi_0[1,1](\omega_n)}. \tag{48}$$

The diagrams involving vertex corrections, such as the one shown in the third line of Figure 1, are of higher order in the $O(1/N_c)$ power-counting scheme. Thus, the computation of the leading-order contribution to the bulk viscosity reduces to the calculation of the series of loop diagrams defined by Equation (47), which in turn requires the evaluation of the single-loop diagram given by Equation (46). To carry out the sum over the Matsubara frequencies in Equation (46) one needs the frequency dependence of the operators $\hat{a}$ and $\hat{b}$ which arises when $\hat{a}, \hat{b} \propto \partial_\tau$ [see Equation (44)]. Indeed, in the frequency space, such dependence translates as $\partial_\tau \to -i\bar{\omega}_l \equiv -i(\omega_l + \omega_n/2)$. For such cases, we separate the $i\bar{\omega}_l$-dependence by formally factorizing the frequency dependence into a function $f(i\bar{\omega}_l)$, i.e., we write $\hat{a}...\hat{b}... = f(i\bar{\omega}_l)\hat{a}_0...\hat{b_0}...$, where $\hat{a}_0$ and $\hat{b}_0$ do not depend on $i\bar{\omega}_l$. After summation over the Matsubara frequencies and subsequent analytical continuation (i.e., $i\omega_n = \omega + i\delta$) we obtain (see Appendix A for details)

$$\Pi_0[\hat{a},\hat{b}](\omega) = \int_{-\infty}^{\infty} d\varepsilon \int_{-\infty}^{\infty} d\varepsilon' \int \frac{d\boldsymbol{p}}{(2\pi)^3} \mathrm{Tr}[\hat{a}_0 A(\boldsymbol{p},\varepsilon')\hat{b}_0 A(\boldsymbol{p},\varepsilon)] \frac{\tilde{n}(\varepsilon')f(\varepsilon' - \omega/2) - \tilde{n}(\varepsilon)f(\varepsilon + \omega/2)}{\varepsilon - \varepsilon' + \omega + i\delta}, \tag{49}$$

where $\tilde{n}(\varepsilon) = n(\varepsilon) - 1/2$ with $n(\varepsilon) = [e^{\beta(\varepsilon-\mu)} + 1]^{-1}$ being the Fermi distribution for quarks. Finally, we separate the real and imaginary parts in Equation (49) by exploiting the Dirac identity

$$\frac{1}{x + i\delta} = P\frac{1}{x} - i\pi\delta(x). \tag{50}$$

From Equations (49) and (50) we find

$$\frac{d}{d\omega}\mathrm{Im}\Pi_0[\hat{a},\hat{b}](\omega)\Big|_{\omega=0} = -\pi\int_{-\infty}^{\infty}d\varepsilon\int\frac{d\boldsymbol{p}}{(2\pi)^3}\frac{\partial n(\varepsilon)}{\partial\varepsilon}f(\varepsilon)\mathrm{Tr}[\hat{a}_0 A(\boldsymbol{p},\varepsilon)\hat{b}_0 A(\boldsymbol{p},\varepsilon)], \tag{51}$$

and

$$\mathrm{Im}\Pi_0[\hat{a},\hat{b}](\omega)\Big|_{\omega=0} = \frac{d}{d\omega}\mathrm{Re}\Pi_0[\hat{a},\hat{b}](\omega)\Big|_{\omega=0} = 0. \tag{52}$$

Using Equation (52) we can compute the imaginary part of Equation (47)

$$\frac{d}{d\omega}\mathrm{Im}\Pi[\hat{a},\hat{b}](\omega)\Big|_{\omega=0} = L_0[\hat{a},\hat{b}] + \bar{G}L_1[\hat{a},\hat{b}] + \bar{G}^2L_2[\hat{a},\hat{b}], \tag{53}$$

where

$$\begin{aligned}
L_0[\hat{a},\hat{b}] &= \frac{d}{d\omega}\mathrm{Im}\Pi_0[\hat{a},\hat{b}](\omega)\Big|_{\omega=0}, && (54)\\
L_1[\hat{a},\hat{b}] &= R_0[\hat{a},1]L_0[1,\hat{b}] + R_0[1,\hat{b}]L_0[\hat{a},1], && (55)\\
L_2[\hat{a},\hat{b}] &= L_0[1,1]R_0[\hat{a},1]R_0[1,\hat{b}], && (56)\\
R_0[\hat{a},\hat{b}] &= \mathrm{Re}\Pi_0[\hat{a},\hat{b}](\omega)\Big|_{\omega=0}, && (57)\\
\bar{G} &= \frac{G}{1-GR_0[1,1]}. && (58)
\end{aligned}$$

To compute the traces in Equations (49) and (51) one needs to exploit the Dirac decomposition of the spectral function

$$A(\boldsymbol{p},p_0) = -\frac{1}{\pi}(mA_s + p_0\gamma_0 A_0 - \boldsymbol{p}\boldsymbol{\gamma}A_v), \tag{59}$$

where m is the quark mass. The coefficients A_s, A_0 and A_v can be expressed in terms of the relevant components of the quark self-energy according to the relations [19,32,33]

$$A_i(p_0,p) = \frac{1}{d}[n_1\varrho_i - 2n_2(1+r_i)], \qquad d = n_1^2 + 4n_2^2, \tag{60}$$

where $\varrho_i = \mathrm{Im}\Sigma_i$, $r_i = \mathrm{Re}\Sigma_i$, $i = s,0,v$, and

$$\begin{aligned}
n_1 &= p_0^2[(1+r_0)^2 - \varrho_0^2] - \boldsymbol{p}^2[(1+r_v)^2 - \varrho_v^2] - m^2[(1+r_s)^2 - \varrho_s^2], && (61)\\
n_2 &= p_0^2\varrho_0(1+r_0) - \boldsymbol{p}^2\varrho_v(1+r_v) - m^2\varrho_s(1+r_s). && (62)
\end{aligned}$$

From now on we will neglect the irrelevant real parts of the self-energy, which lead to momentum-dependent corrections to the constituent quark mass in next-to-leading order $\mathcal{O}(N_c^{-1})$ and will keep only the imaginary parts which were computed in Refs. [19,32,33]. The three components of the quark self-energy are identified via

$$\Sigma^{R(A)} = m\Sigma_s^{(*)} - p_0\gamma_0\Sigma_0^{(*)} + \boldsymbol{p}\boldsymbol{\gamma}\Sigma_v^{(*)}. \tag{63}$$

With this input, we can now calculate the relevant correlators entering Equation (44). Computing the traces and performing the angular integrations in Equations (49) and (51), we find, e.g.,

$$R_0\,[1, i\gamma_1\partial_1] = -\frac{2N_cN_f}{3\pi^4}\int_{-\infty}^{\infty}d\varepsilon\int_{-\infty}^{\infty}d\varepsilon'\int_0^{\Lambda}dp\frac{n(\varepsilon)-n(\varepsilon')}{\varepsilon-\varepsilon'}mp^4(A_s'A_v+A_sA_v'), \tag{64}$$

$$L_0[i\gamma_1\partial_1, i\gamma_1\partial_1] = -\frac{2N_cN_f}{15\pi^3}\int_{-\infty}^{\infty}d\varepsilon\int_0^{\Lambda}dp\frac{\partial n(\varepsilon)}{\partial\varepsilon}p^4(-5m^2A_s^2+5\varepsilon^2A_0^2+p^2A_v^2), \tag{65}$$

where $A_i' \equiv A_i(\boldsymbol{p}, \varepsilon')$; $N_c = 3$ and $N_f = 2$ are the color and flavor numbers, respectively. The remaining correlation functions can be computed in analogy to Equations (64) and (65); the explicit expressions are given in Ref. [16].

Inserting the relevant correlators in Equations (37), (44), (53)–(58), we can write the bulk viscosity as

$$\zeta = \zeta_0 + \zeta_1 + \zeta_2, \tag{66}$$

where each of the three terms arises from the corresponding terms in Equation (53). The first (single-loop) term is given by

$$\zeta_0 = -\frac{2N_cN_f}{9\pi^3}\int_{-\infty}^{\infty}d\varepsilon\frac{\partial n}{\partial\varepsilon}\int_0^{\Lambda}dpp^2\Big[2(ax+by+cz)^2-(x^2-y^2+z^2)(a^2-b^2+c^2)\Big], \tag{67}$$

where $x = 3(1+\gamma)m_0$, $y = 3(\delta-\varepsilon)$, $z = (2+3\gamma)p$, $a = mA_s$, $b = \varepsilon A_0$, and $c = pA_v$. The multiloop contributions are given by

$$\zeta_1 = 2(\bar{G}\bar{R})I_1, \qquad \zeta_2 = (\bar{G}\bar{R})^2I_2, \tag{68}$$

where the effective coupling $\bar{G}$ is given by

$$\bar{G} = \frac{G}{1-R_0G}, \tag{69}$$

with the polarization loop

$$R_0 = -\frac{2N_cN_f}{\pi^4}\int_{-\infty}^{\infty}d\varepsilon\int_{-\infty}^{\infty}d\varepsilon'\frac{n(\varepsilon)-n(\varepsilon')}{\varepsilon-\varepsilon'}\int_0^{\Lambda}dpp^2(aa'+bb'-cc'), \tag{70}$$

and

$$I_1 = -\frac{2N_cN_f}{3\pi^3}\int_{-\infty}^{\infty}d\varepsilon\frac{\partial n}{\partial\varepsilon}\int_0^{\Lambda}dpp^2\Big[x(a^2+b^2-c^2)+2a(by+cz)\Big], \tag{71}$$

$$I_2 = -\frac{2N_cN_f}{\pi^3}\int_{-\infty}^{\infty}d\varepsilon\frac{\partial n}{\partial\varepsilon}\int_0^{\Lambda}dpp^2(a^2+b^2-c^2), \tag{72}$$

$$\bar{R} = -\frac{2N_cN_f}{3\pi^4}\int_{-\infty}^{\infty}d\varepsilon\int_{-\infty}^{\infty}d\varepsilon'\int_0^{\Lambda}dpp^2\frac{1}{\varepsilon-\varepsilon'}\Big\{[n(\varepsilon)-n(\varepsilon')]$$
$$\times\ \big[x(aa'+bb'-cc')+z(a'c+ac')\big]+\Big[yn(\varepsilon)-y'n(\varepsilon')+\frac{3}{2}(\varepsilon-\varepsilon')\Big](a'b+ab')\Big\}. \tag{73}$$

Here the functions a', b', c', y' are obtained from a, b, c, y defined above by substitution $\varepsilon \to \varepsilon'$. Equations (66)–(73) express the bulk viscosity of quark plasma in terms of the components of its spectral function.

It is remarkable that the multiloop contributions to the bulk viscosity vanish trivially in the chirally symmetric case, where $m_0 = 0$. Indeed, for massless quarks and temperatures $T > T_c$, where T_c is the critical temperature of the chiral phase transition, we find $x = 0$ and $a, a' \propto m = 0$ in Equation (70). As a result, we have $\zeta_{1,2} = 0$ and $\zeta = \zeta_0$ according to Equations (68) and (66).

4. Numerical Results

We use the Lorentz components of the quark spectral function, obtained previously in Refs. [19,32,33], to evaluate numerically the bulk viscosity. We concentrate on the region of the phase diagram which is located above the Mott transition temperature $T_{\rm M}$, which is defined as the threshold temperature at any given chemical potential above which the meson decay into two on-mass-shell quarks is kinematically allowed. It is identical to the chiral phase transition temperature T_c in the chiral limit $m_0 = 0$.

To gain insight into the numerical results for the bulk viscosity, it is useful first to analyze the integrands of Equations (67) and (70)–(73). The integrands of ζ_0, I_1 and I_2 are shown in Figure 2. Each of these integrands develops a peak structure at $p \simeq |\varepsilon|$, whereby the height of the peak rapidly increases with $|\varepsilon|$. The momentum integrals are increasing functions of $|\varepsilon|$ as long as $|\varepsilon| \leq \Lambda$, and decreasing for larger energies (because of the momentum cut-off $p \leq \Lambda$, see Figure 2).

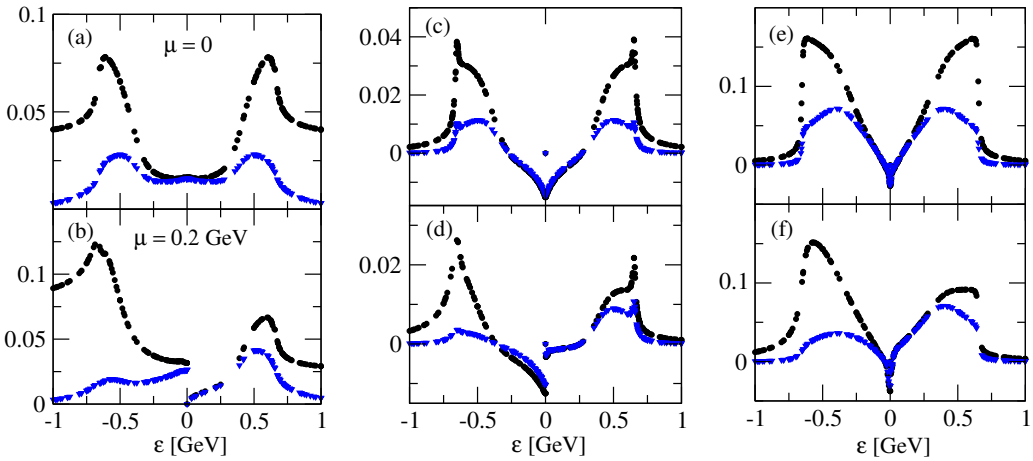

Figure 2. The integrands of ζ_0 (**a**,**b**), I_1 (**c**,**d**) and I_2 (**e**,**f**) as functions of the quark energy without (black circles, in GeV units) and with (blue triangles) the factor $-\partial n/\partial\varepsilon$ for vanishing (**a**,**c**,**e**) and finite (**b**,**d**,**f**) chemical potential. The temperature is fixed at $T = 0.26$ GeV.

Note that for $\mu = 0$ the integrands are even functions of ε, which reflects the quark-antiquark symmetry. The factor $\partial n(\varepsilon)/\partial\varepsilon$ breaks this symmetry for non-vanishing chemical potentials by increasing the contribution of quarks. Thus, we see that the dominant contribution to the bulk viscosity comes from the modes with $p \simeq |\varepsilon|$, whereby the quark contribution dominates the antiquark contribution at non-zero μ.

Now we turn to the three-dimensional integrals R_0 and $\bar{R}$ given by Equations (70) and (73). Their integrands are strongly peaked at $p \simeq |\varepsilon| \simeq |\varepsilon'|$, and have two smaller maxima located at $p \simeq |\varepsilon|$ and $p \simeq |\varepsilon'|$ in the cases where $|\varepsilon| \neq |\varepsilon'|$, see Figure 3. As a result, the momentum integrals of these expressions obtain the main contribution form energies $\varepsilon' \simeq \pm\varepsilon$. We also observe that the height of each peak increases with $|\varepsilon|$ for $|\varepsilon| \leq \Lambda$ and sharply drops beyond the cut-off. The peak structures seen above reflect the quasiparticle-like nature of the excitations, which however have non-zero width because of the meson decay and recombination processes included in our consideration.

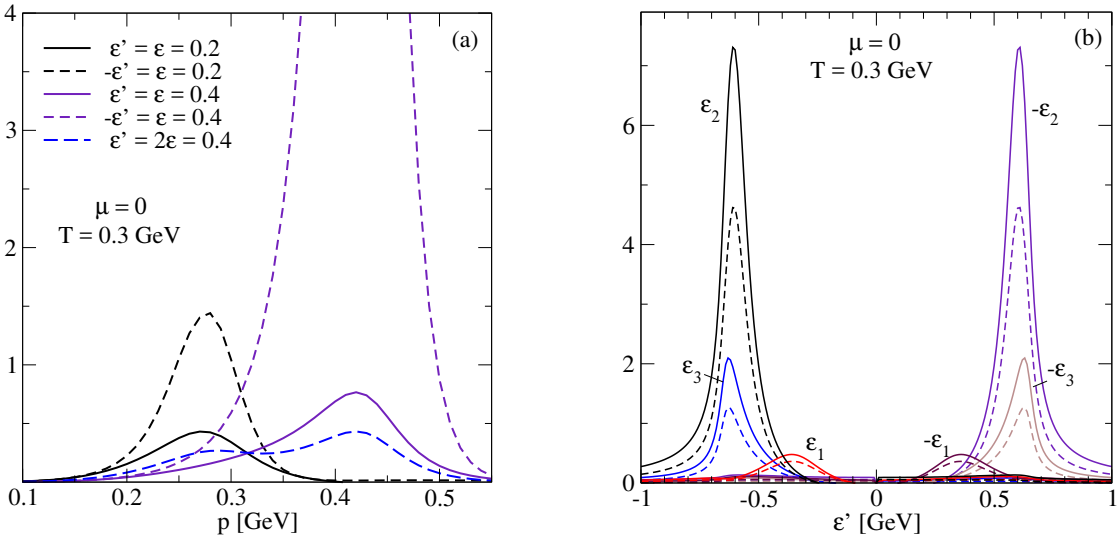

Figure 3. The integrands of the integral R_0: (**a**) the inner integrand as a function of quark momentum at various values of ε and ε' (shown in GeV units); (**b**) the p-integral of R_0 (solid lines, in GeV units) and its product with the factor $[n(\varepsilon) - n(\varepsilon')]/(\varepsilon - \varepsilon')$ (dashed lines) as functions of ε' for various values of ε: $\varepsilon_1 = 0.3$, $\varepsilon_2 = 0.6$ and $\varepsilon_3 = 0.7$ GeV.

Figure 4 illustrates the temperature and chemical potential dependence of the integrals I_1, I_2, R_0 and the renormalized coupling $\bar{G} = G/(1 - GR_0)$ [given by Equation (58)]. The behavior of $\bar{R}$ is similar to R_0 and is not shown. Quantitatively, the three- and two-dimensional integrals R_0 and I_1, I_2, respectively, show the same behavior, reflecting the importance of the meson decay processes close to the Mott line. The renormalized coupling $\bar{G}$ attains its maximum close to the Mott line, where it exceeds the bare coupling constant roughly by an order of magnitude. Because of this behavior of $\bar{G}$, the multiloop contributions to the bulk viscosity given by Equation (68) are expected to be important close to the Mott temperature.

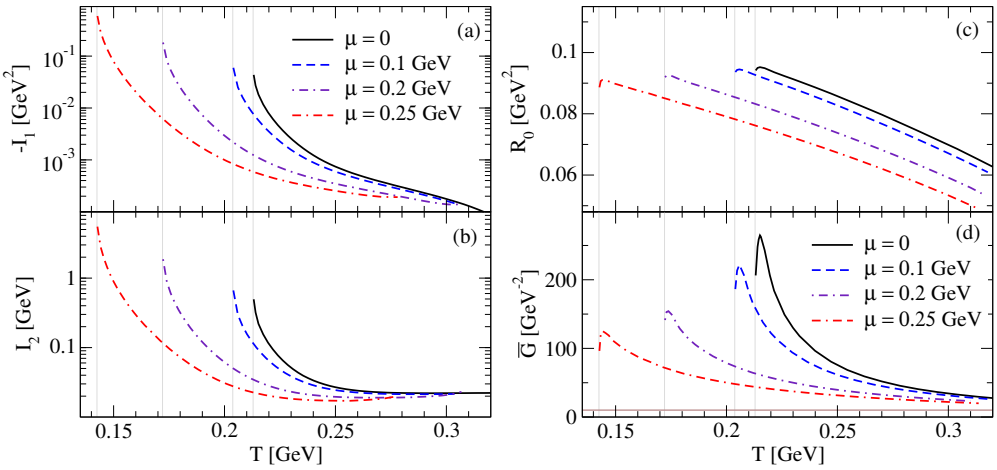

Figure 4. Dependence of the integrals I_1 (**a**), I_2 (**b**), R_0 (**c**) and the renormalized coupling $\bar{G}$ (**d**) on the temperature for several values of the chemical potential. The corresponding Mott lines are shown by vertical lines. The value of the bare coupling constant G is shown by the solid horizontal line.

The results for the bulk viscosity are shown in Figure 5. The multiloop contributions ζ_1 and ζ_2 dominate over the one-loop contribution ζ_0 in the regime close to the Mott transition line, where all three components rapidly decrease with the temperature and density. At high enough temperatures,

the one-loop contribution scales as T^3 and dominates over the multiloop contributions. The net bulk viscosity which is the sum of the one-loop and multiloop contributions then exhibits a shallow minimum as a function of temperature. From the analysis above, we thus conclude that the single-loop approximation is justified only at sufficiently high temperatures where multiloop diagrams are suppressed.

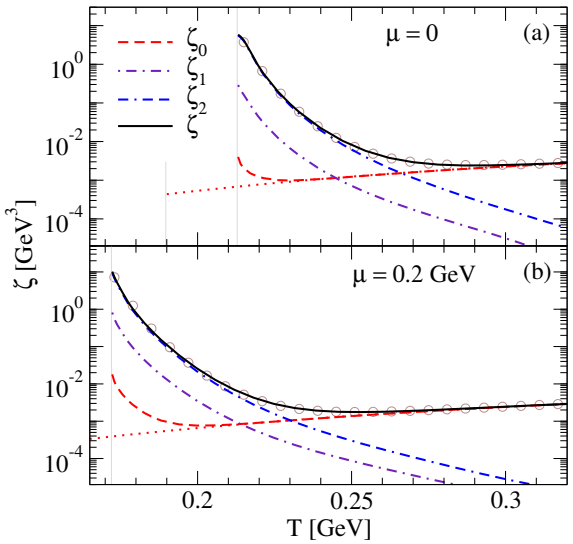

Figure 5. The contributions of the single-loop (ζ_0) and multiloop (ζ_1, ζ_2) diagrams to the bulk viscosity, as well as their sum as functions of the temperature for vanishing (**a**) and finite (**b**) chemical potential. The dotted lines correspond to the chiral limit $m_0 = 0$. The results of the fit formula (74) are shown by circles.

We now comment briefly on the case where the chiral symmetry is intact, i.e., $m_0 = 0$. In this case, the multiloop contributions vanish automatically, as explained in Section 3. The bulk viscosity is then given by the single-loop contribution ζ_0 taken in the limit $m \to 0$, which is shown in Figure 5 by the dotted lines for zero and finite chemical potentials. Contrary to the case where $m_0 \neq 0$, here ζ_0 is smooth at the Mott temperature and increases with the temperature $\propto T^3$ in the whole temperature-density range. We thus conclude that the *explicit* chiral symmetry breaking is essential for the correct description of the bulk viscosity in the low-temperature region of the phase diagram, especially in the region close to the chiral phase transition line.

For completeness, we also compare our results with the shear viscosity η, which was computed previously in Ref. [19] (see also Refs. [32,33]) by employing the same formalism and approximations. Figure 6 shows the dependence of the ratios ζ/s and η/s, where s is the entropy density, on the temperature for several values of the chemical potential [16,19]. For comparison, we also show the AdS/CFT lower bound $1/4\pi$ on the η/s ratio [2]. We see that both ratios decrease rapidly with the temperature, but the slope of this decrease is larger in the case of the bulk viscosity in the region which is close to the Mott transition line. In this regime, the bulk viscosity exceeds the shear viscosity by factors $\zeta/\eta \simeq 5 \div 20$. Thus, in the low-temperature regime close to the Mott transition line the bulk viscosity is the dominant source of dissipation. It is worth stressing that had we kept only the one-loop contribution to the bulk viscosity, it would have been negligible compared to the shear viscosity. As ζ drops much faster than η with the temperature, the shear viscosity is the dominant dissipation channel at high temperatures.

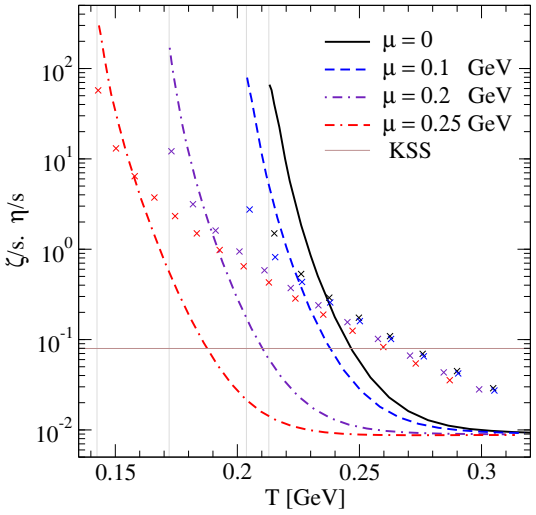

Figure 6. The ratio ζ/s as a function of the temperature for several values of the chemical potential. The corresponding η/s ratios are shown for comparison by crosses. The solid horizontal line shows the KSS bound [2].

Our numerical results can be fitted using the formula

$$\zeta_{\rm fit}(T,\mu) = a(y)\exp\left[\frac{c(y)}{T/T_M(y) - b(y)}\right] + d(y)T^3, \tag{74}$$

where $y = \mu/\mu_0$, and $\mu_0 = 0.345$ GeV is the value of the chemical potential at which the Mott line terminates. The coefficients a, b, c, d depend only on the chemical potential and are given by

$$a(y) = (2.57 - 5.65y^2) \times 10^{-6}\ [\mathrm{GeV}^3], \tag{75}$$
$$b(y) = 0.806 - 0.055y^2 - 0.617y^4, \tag{76}$$
$$c(y) = 2.89 + 0.96y^2 + 12.73y^4, \tag{77}$$
$$d(y) = 0.082 + 0.02y^2. \tag{78}$$

The relative error of the fit formula (74) is $\leq 10\%$ for chemical potentials $\mu \leq 0.2$ GeV. The bulk viscosity according to our fit formula is shown in Figure 5 by empty circles. The fit formula above should be complemented by a fit to the Mott temperature as a function of the chemical potential, which is given by the formula

$$T_{\rm M}^{\rm fit}(\mu) = T_0 \begin{cases} 1 - \sqrt{\gamma y} e^{-\pi/(\gamma y)} & 0 \leq y \leq 0.5, \\ \sqrt{1.55(1-y) + 0.04(1-y)^2} & 0.5 < y \leq 1, \end{cases} \tag{79}$$

where $T_0 = T_{\rm M}(\mu = 0) = 0.213$ GeV, and $\gamma = 2.7$. The relative accuracy of the formula (79) is $\leq 3\%$ for chemical potentials $\mu \leq 0.32$ GeV.

5. Conclusions

In this contribution, we provided a general derivation of the Kubo formula for the bulk viscosity from Zubarev's formalism of NESO generalized to systems with multiple conserved charges. The method was then illustrated on the example of computation of the bulk viscosity of quark matter in the framework of the two-flavor NJL model. The previous discussion of Ref. [16] has been supplemented by further details.

The key finding of our work is that at low temperatures and close to the Mott transition line the overall multiloop contribution to the bulk viscosity is larger than the one-loop contribution. This is

in contrast to the results found for the shear viscosity and the thermal and electrical conductivities, for which the single-loop approximation gives the leading-order result [19]. We have shown that the bulk viscosity decreases with the temperature and the chemical potential in this regime, attains a minimum and then increases again at higher temperatures where the one-loop contribution becomes dominant.

Phenomenologically interesting is the fact that the bulk viscosity provides the main source of dissipation of stresses close to the Mott line as it exceeds the shear viscosity in this regime by factors of $5 \div 20$. The bulk viscosity drops faster than the shear viscosity as the temperature increases and it becomes negligible above a certain value of the temperature. Finally, we observed that in the chiral symmetric case, where the quark masses vanish above the (critical) Mott temperature, the picture is different. In this case, the multiloop contributions to the bulk viscosity vanish, and consequently the bulk viscosity becomes negligible compared to the shear viscosity in the entire temperature-density plane.

Author Contributions: Conceptualization, A.H., A.S.; Methodology, A.H., A.S.; Investigation, A.H., A.S.; Writing—Original Draft Preparation, A.H., A.S.; Writing—Review & Editing, A.H., A.S.; Funding Acquisition, A.S.

Funding: This research was funded by Deutsche Forschungsgemeinschaft, grant number SE 1836/4-1 and by European Cooperation in Science and Technology (Actions MP1304 and CA16214).

Acknowledgments: We are grateful to Xu-Guang Huang and Dirk H. Rischke for discussions. A.H. acknowledges support from the HGS-HIRe graduate program at Goethe University. A.S. was supported by the Deutsche Forschungsgemeinschaft (Grant No. SE 1836/4-1). The support from European COST Actions "NewCompStar" (MP1304) and "PHAROS" (CA16214) and the LOEWE-Program of Helmholtz International Center for FAIR of the state of Hesse (Germany) is gratefully acknowledged.

Conflicts of Interest: The authors declare no conflict of interest.

Appendix A. Matsubara Summations

To perform the Matsubara summation in Equation (46) we express the full quark propagator in terms of the quark spectral function

$$D(\boldsymbol{p}, z) = \int_{-\infty}^{\infty} d\varepsilon \frac{A(\boldsymbol{p}, \varepsilon)}{z - \varepsilon}, \tag{A1}$$

where the spectral function is defined as

$$A(\boldsymbol{p}, \varepsilon) = -\frac{1}{2\pi i} \left[D^R(\boldsymbol{p}, \varepsilon) - D^A(\boldsymbol{p}, \varepsilon) \right], \tag{A2}$$

with $D^{R/A}(\boldsymbol{p}, \varepsilon)$ being the retarded/advanced Green's functions. According to Equation (A1), $D(\boldsymbol{p}, z)$ has a branch cut on the real axis, therefore a calculation of the residues gives for the integrand of Equation (46)

$$\begin{aligned} S[\hat{a}, \hat{b}](\boldsymbol{p}, i\omega_n) &\equiv T \sum_l \mathrm{Tr}\left[\hat{a} D(\boldsymbol{p}, i\omega_l + i\omega_n) \hat{b} D(\boldsymbol{p}, i\omega_l)\right] \\ &= T \sum_l f(i\bar{\omega}_l) \mathrm{Tr}\left[\hat{a}_0 D(\boldsymbol{p}, i\omega_l + i\omega_n) \hat{b}_0 D(\boldsymbol{p}, i\omega_l)\right] \\ &= -\int_C \frac{dz}{2\pi i} \tilde{n}(z) f(z + i\omega_n/2) \mathrm{Tr}\left[\hat{a}_0 D(\boldsymbol{p}, z + i\omega_n) \hat{b}_0 D(\boldsymbol{p}, z)\right], \end{aligned} \tag{A3}$$

where $n(z) = [e^{\beta(z-\mu)} + 1]^{-1}$ is the Fermi distribution function, and $\tilde{n}(z) = n(z) - 1/2$. The integration contour C is shown in Figure A1, where the circle should be taken infinitely large in order to include all poles of the function $n(z)$. Note that due to the fact that ω_n does not coincide with ω_l for any n and l, the poles of $n(z)$ do not lie on the branch cuts of C.

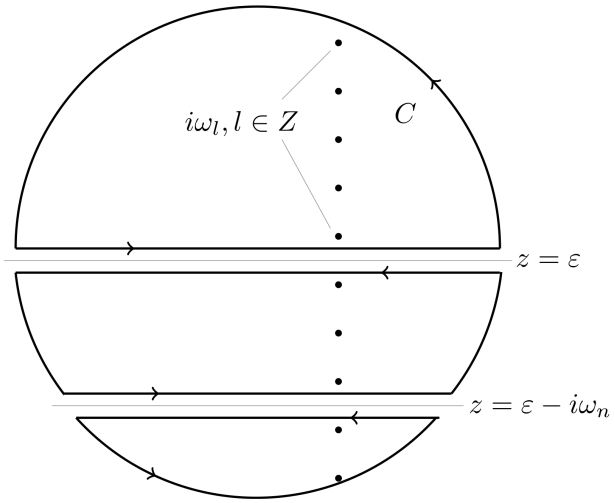

Figure A1. The contour of integration in Equation (A3). The dots correspond to the fermionic Matsubara frequencies.

We show now that the contribution of the large circle to the integral (A3) vanishes. Because of the sum rule $\int_{-\infty}^{\infty} d\varepsilon A(\boldsymbol{p},\varepsilon) = \text{const}$, the quark propagator for large $|z|$ has the scaling $D \propto z^{-1}$. Therefore, for large $|z|$ the integrand in Equation (A3) scales as $\propto \tilde{n}(z) z^{k-2}$ (recall that $f \propto z^k$). For the Fermi distribution function we have the asymptotics $n(z) \to_{\mathrm{Re}z\to\infty} 0$ and $n(z) \to_{\mathrm{Re}z\to-\infty} 1$. Substituting $z = Re^{i\phi}$, $dz = iRe^{i\phi}d\phi$, and performing the limit $R \to \infty$, we can write for the integral along the circle

$$\begin{aligned} S_R \propto -\int_{C_R} \frac{dz}{2\pi i} z^{k-2}\tilde{n}(z) &= \frac{R^{k-1}}{4\pi}\left[\int_{-\pi/2}^{\pi/2} d\phi e^{i(k-1)\phi} - \int_{\pi/2}^{3\pi/2} d\phi e^{i(k-1)\phi}\right] \\ &= \frac{R^{k-1}}{\pi}\begin{cases} \frac{\sin(k-1)\pi/2}{k-1}, & k \neq 1, \\ 0, & k = 1. \end{cases} \end{aligned} \tag{A4}$$

As seen from Equation (A4), the integral vanishes in the limit $R \to \infty$ if $k = 0, 1$. If $k = 2$, we have $S_R \propto R \to \infty$, which is purely real and can be dropped since in this case we need only the imaginary parts of $S[f]$ functions. As a result, we need to keep only the integrals along the two branch cuts shown in Figure A1. Then, using also Equation (A2), we obtain for Equation (A3)

$$\begin{aligned} S[\hat{a},\hat{b}](\boldsymbol{p}, i\omega_n) = \int_{-\infty}^{\infty} d\varepsilon \tilde{n}(\varepsilon)\Big\{ & f(\varepsilon - i\omega_n/2)\mathrm{Tr}[\hat{a}_0 A(\boldsymbol{p},\varepsilon)\hat{b}_0 D(\boldsymbol{p},\varepsilon - i\omega_n)] \\ & + f(\varepsilon + i\omega_n/2)\mathrm{Tr}[\hat{a}_0 D(\boldsymbol{p},\varepsilon + i\omega_n)\hat{b}_0 A(\boldsymbol{p},\varepsilon)]\Big\}, \end{aligned} \tag{A5}$$

where we took into account that $n(\varepsilon - i\omega_n) = n(\varepsilon)$. Substituting the spectral representation (A1) into Equation (A5), changing the variables $\varepsilon \leftrightarrow \varepsilon'$ in the first term and performing analytical continuation via $i\omega_n \to \omega + i\delta$, we find

$$S[\hat{a},\hat{b}](\boldsymbol{p},\omega) = \int_{-\infty}^{\infty} d\varepsilon \int_{-\infty}^{\infty} d\varepsilon' \ \mathrm{Tr}[\hat{a}_0 A(\boldsymbol{p},\varepsilon')\hat{b}_0 A(\boldsymbol{p},\varepsilon)] \frac{\tilde{n}(\varepsilon) f(\varepsilon + \omega/2) - \tilde{n}(\varepsilon') f(\varepsilon' - \omega/2)}{\varepsilon - \varepsilon' + \omega + i\delta}. \tag{A6}$$

Substituting this expression into Equation (46), we obtain Equation (49) of the main text.

References

1. Danielewicz, P.; Gyulassy, M. Dissipative phenomena in quark-gluon plasmas. *Phys. Rev. D* **1985**, *31*, 53–62. [CrossRef]
2. Kovtun, P.; Son, D.; Starinets, A. Viscosity in Strongly Interacting Quantum Field Theories from Black Hole Physics. *Phys. Rev. Lett.* **2005**, *94*, 111601. [CrossRef] [PubMed]
3. Hosoya, A.; Kajantie, K. Transport coefficients of QCD matter. *Nucl. Phys. B* **1985**, *250*, 666–688. [CrossRef]
4. Arnold, P.; Doğan, Ç.; Moore, G.D. Bulk viscosity of high-temperature QCD. *Phys. Rev. D* **2006**, *74*, 085021. [CrossRef]
5. Moore, G.; Saremi, O. Bulk viscosity and spectral functions in QCD. *Phys. Rev. D* **2008**, *9*, 015. [CrossRef]
6. Chen, J.-W.; Liu, Y.-F.; Song, Y.-K.; Wang, Q. Shear and bulk viscosities of a weakly coupled quark gluon plasma with finite chemical potential and temperature: Leading-log results. *Phys. Rev. D* **2013**, *87*, 036002. [CrossRef]
7. Meyer, H. Calculation of the Bulk Viscosity in $SU(3)$ Gluodynamics. *Phys. Rev. D* **2008**, *100*, 162001. [CrossRef] [PubMed]
8. Paech, K.; Pratt, S. Origins of bulk viscosity in relativistic heavy ion collisions. *Phys. Rev. C* **2006**, *74*, 014901. [CrossRef]
9. Karsch, F.; Kharzeev, D.; Tuchin, K. Universal properties of bulk viscosity near the QCD phase transition. *Phys. Lett. B* **2008**, *663*, 217–221. [CrossRef]
10. Aarts, G. Transport and spectral functions in high-temperature QCD. *arXiv* **2007**, arXiv:0710.0739.
11. Sasaki, C.; Redlich, K. Transport coefficients near chiral phase transition. *Nucl. Phys. A* **2010**, *832*, 62–75. [CrossRef]
12. Chakraborty, P.; Kapusta, J. Quasiparticle theory of shear and bulk viscosities of hadronic matter. *Phys. Rev. C* **2011**, *83*, 014906. [CrossRef]
13. Chandra, V. Bulk viscosity of anisotropically expanding hot QCD plasma. *Phys. Rev. D* **2011**, *84*, 09402. [CrossRef]
14. Dobado, A.; Llanes-Estrada, F.; Torres-Rincon, J. Bulk viscosity and energy-momentum correlations in high energy hadron collisions. *Eur. Phys. J. C* **2012**, *72*, 1873. [CrossRef]
15. Marty, R.; Bratkovskaya, E.; Cassing, W.; Aichelin, J.; Berrehrah, H. Transport coefficients from the Nambu-Jona-Lasinio model for $SU(3)_f$. *Phys. Rev. C* **2013**, *88*, 045204. [CrossRef]
16. Harutyunyan, A.; Sedrakian, A. Bulk viscosity of two-flavor quark matter from the Kubo formalism. *Phys. Rev. D* **2017**, *96*, 034006. [CrossRef]
17. Xiao, S.-S.; Guo, P.-P.; Zhang, L.; Hou, D.-F. Bulk viscosity of hot dense Quark matter in the PNJL model. *Chin. Phys. C* **2014**, *38*, 054101. [CrossRef]
18. Ghosh, S.; Peixoto, T.; Roy, V.; Serna, F.; Krein, G. Shear and bulk viscosities of quark matter from quark-meson fluctuations in the Nambu-Jona-Lasinio model. *Phys. Rev. C* **2016**, *93*, 045205. [CrossRef]
19. Harutyunyan, A.; Rischke, D.H.; Sedrakian, A. Transport coefficients of two-flavor quark matter from the Kubo formalism. *Phys. Rev. D* **2017**, *95*, 114021. [CrossRef]
20. Zubarev, D. *Nonequilibrium Statistical Thermodynamics*; Studies in Soviet Science; Consultants Bureau: New York, NY, USA, 1974.
21. Zubarev, D.; Morozov, V.; Röpke, G. *Statistical Mechanics of Nonequilibrium Processes*; Akademie Verlag: Berlin, Germany, 1996.
22. Quack, E.; Klevansky, S. Effective $1/N_c$ expansion in the Nambu-Jona-Lasinio model. *Phys. Rev. C* **1994**, *49*, 3283–3288. [CrossRef]
23. Hosoya, A.; Sakagami, M.A.; Takao, M. Nonequilibrium thermodynamics in field theory: Transport coefficients. *Ann. Phys.* **1984**, *154*, 229–252. [CrossRef]
24. Huang, X.G.; Sedrakian, A.; Rischke, D.H. Kubo formulas for relativistic fluids in strong magnetic fields. *Ann. Phys.* **2011**, *326*, 3075–3094. [CrossRef]
25. Landau, L.; Lifshitz, E. *Fluid Mechanics*; Butterworth-Heinemann: Oxford, UK, 1987.
26. Eckart, C. The Thermodynamics of Irreversible Processes. III. Relativistic theory of the simple fluid. *Phys. Rev.* **1940**, *58*, 919–924. [CrossRef]
27. Zubarev, D.; Tishchenko, S. Nonlocal hydrodynamics with memory. *Physica* **1972**, *59*, 285–304. [CrossRef]
28. Mori, H. Statistical-Mechanical Theory of Transport in Fluids. *Phys. Rev.* **1958**, *112*, 1829–1842. [CrossRef]

29. Dusling, K.; Schäfer, T. Bulk viscosity, particle spectra, and flow in heavy-ion collisions. *Phys. Rev. C* **2012**, *85*, 044909. [CrossRef]
30. Jeon, S. Hydrodynamic transport coefficients in relativistic scalar field theory. *Phys. Rev. D* **1995**, *52*, 3591–3642. [CrossRef]
31. De Groot, S.; Mazur, P. *Non-Equilibrium Thermodynamics*; North-Holland Publishing Company: Amsterdam, The Netherlands, 1962.
32. Lang, R.; Kaiser, N.; Weise, W. Shear viscosities from Kubo formalism in a large-N_c Nambu–Jona-Lasinio model. *Eur. Phys. J. A* **2015**, *51*, 127. [CrossRef]
33. Lang, R.; Weise, W. Shear viscosity from Kubo formalism: NJL model study. *Eur. Phys. J. A* **2014**, *50*, 63. [CrossRef]